Broadband Tissue-Equivalent Phantom for BAN Applications at Millimeter Waves

Nacer Chahat, *Student Member, IEEE*, Maxim Zhadobov, *Member, IEEE*, and Ronan Sauleau, *Senior Member, IEEE*

***Abstract*—The extension of body area networks from microwaves to millimeter waves requires to develop experimental phantoms emulating the dielectric properties of human skin for the accurate, reproducible, and well-controlled characterization of wearable antennas, on-body propagation channel, and absorption of the electromagnetic power by the human body. Here we introduce a broadband skin-equivalent semisolid phantom whose composition is optimized to coincide with measured values of the human skin permittivity in the 55–65-GHz range. To confirm the accuracy of this phantom, specific absorption rate measurements are performed at 60 GHz using a temperature-based approach. An excellent agreement between the experimental and numerical results is demonstrated.**

***Index Terms*—Body-area network (BAN), body-centric wireless communications, experimental phantom, millimeter waves (MMWs), specific absorption rate (SAR).**

I. Introduction

BODY-CENTRIC wireless communication systems refer to wireless networking between wearable and/or implanted sensors and another sensor located on, off, or in the body. Near-future applications include personal healthcare, entertainment, identification systems, sport, smart home, space, and military applications [1], [2]. Several studies have been conducted in various directions, including the design and optimization of on- and off-body wearable antennas [3]–[7], the characterization of the on-body channel [8], the analysis of the effects of the human body on wireless links [9], [10], and on-body diversity studies [11]. Although wearable antennas for body area networks (BANs) have been characterized on the body up to 17 GHz [12], most of the research works have been focused on industrial–scientific–medical (ISM) bands at 2.45 GHz [13] and 5.5 GHz [14], and on ultra-wideband (UWB) applications [5], [6]. At these frequencies, the on-body channel has been characterized extensively, e.g., [1], [6], [8], [15].

Manuscript received April 03, 2012; accepted April 06, 2012. Date of publication May 16, 2012; date of current version June 26, 2012. This work was supported by the Agence Nationale de la Recherche (ANR) under Grant ANR-09-RPDOC-003-01 (Bio-CEM Project) and Grant ANR-09-VERS-003 (METAVEST Project), and by the Centre National de la Recherche Scientifique (CNRS).

The authors are with the Institute of Electronics and Telecommunications of Rennes (IETR), Unité Mixte de Recherche (UMR), Centre National de la Recherche Scientifique (CNRS) 6164, University of Rennes 1, 35042 Rennes, France (e-mail: nacer.chahat@univ-rennes1.fr).

Color versions of one or more of the figures in this paper are available online at http://ieeexplore.ieee.org.

Digital Object Identifier 10.1109/TMTT.2012.2195196

Although many innovations for on-body communication technologies have emerged recently, it is still not possible to reach very high data rates. Developing BAN in the 60-GHz band is considered as a promising solution to overcome this limitation. This solution also offers several advantages compared to BAN at lower frequencies [16], namely, (1) confidentiality and low interference with neighboring networks due to the oxygen resonance around 60 GHz, and (2) reduced size of the on-body equipment. Recently, two 60-GHz antennas for on-body communications have been introduced [17], [18]. The interactions of millimeter waves (MMWs) with the human body have been also reviewed in [19].

In order to experimentally evaluate the performance of on-body antenna systems in V-band, it is necessary to develop appropriate tissue-equivalent phantoms. Such phantoms can also be used to investigate the on-body channel in a reproducible and well-controlled manner. Recent studies have demonstrated that accurate realistic phantoms are crucial for the reliable characterization of the body-centric propagation channel at 60 GHz [20]. Indeed, the close proximity of an antenna with the human body may result in significant changes in the input impedance, radiation patterns, and antenna efficiency. Besides, measuring the energy absorption induced in real human bodies by on-body antennas is very challenging and involves some ethical issues. Furthermore, the experimental results might fluctuate due to the morphological inter-individual differences and variations of the dielectric properties of biological tissues, inducing thereby reproducibility problems [21]. Moreover, replacing the human body by a phantom is very convenient to measure radiation patterns and enables to overcome feeding problems, thereby facilitating on-body characterization [5].

At frequencies below 10 GHz, three types of experimental phantoms have been considered, namely, the liquid, semisolid, and solid ones. First, liquid phantoms require a container to hold the fluid, which does not allow the measurement of the specific absorption rate (SAR) on the phantom surface. They are well suited for measurements in the 30-MHz–6-GHz range [1], [22] but cannot be used at millimeter range because of the shell. Semisolid phantoms then do not require any bounding container and have been used for antenna and on-body channel characterization. Today, they are available for frequencies below 3 GHz (muscle, brain, and skin phantom) [23] and also cover the 3.1–10.6-GHz band (2/3 muscle equivalent phantom) [24]. Besides, a skin equivalent phantom has been introduced recently at 10 GHz [25]. Finally, solid phantoms can be designed to fit a wide range of complex permittivities [26], [27]. Compared to liquid and semisolid phantoms, solid phantoms provide longer life span with stable dielectric and mechanical

properties over a long time. However, such phantoms are expensive and require special and expensive equipment, along with specific high-temperature (∼260 °C) and high-pressure manufacturing procedures.

The main purpose of this work is to propose an experimental skin-equivalent phantom mimicking accurately the dielectric properties of the human body surface in the 55–65-GHz range. The composition of the phantom was briefly outlined in [28]. In this paper, the fabrication procedure is detailed and critical steps are discussed. Besides, the optimization procedure of its dielectric properties is explained in detail. The influence of variations of the skin permittivity on the reflection/transmission, PD, and SAR is quantitatively investigated. Furthermore, the phantom is experimentally validated trough a dosimetric study. It is demonstrated that the phantom can be used as an accurate experimental model for the power absorption and SAR measurements, representing a very convenient alternative to the direct measurements on the skin [29].

This paper is organized as follows. In Section II, we describe the experimental setup implemented to measure the skin and phantom permittivity. The measured complex permittivity values of the human skin are provided from 55 to 65 GHz. The fabrication and characterization procedures of the proposed semisolid phantom are detailed in Section III. Its dielectric properties are validated by measurements, and results of the SAR measurements are given in Section IV. Finally, conclusions are drawn in Section V.

II. Measurements of the Human Skin Permittivity

As more than 90% of the energy transmitted to the human body is absorbed by skin at 60 GHz [19], it is necessary to determine the dielectric properties of the human skin in order to build 60-GHz equivalent phantoms. In this section, we summarize the data available in the literature and provide new experimental results.

A. Review of the Skin Permittivity Data at MMWs

In contrast to frequencies below 20 GHz, the already-existing data on the relative permittivity of human tissues at MMWs is very limited. In addition, the results reported thus far in the literature strongly depend on the measurement technique, the sample type (*in vivo* or *in vitro* study), and other experimental conditions such as skin temperature, location on the body, and thickness of different skin layers.

Gandhi and Riazi [30] and Alabaster [31] performed *in vitro* measurements. The results presented by Gandhi and Riazi at 60 GHz [30] were obtained using a Debye model relying on measurements performed on rabbit skin at 23 GHz, whereas Alabaster used a free-space technique on excised samples of skin at 60 GHz [31].

Gabriel *et al.* [32] reported extrapolated complex permittivity values up to 110 GHz based on *in vivo* human skin measurements performed below 20 GHz. They reported two skin models, namely, *wet skin* and *dry skin*. For the *wet skin* data, they used a gel to moisture the skin. Human skin under normal environmental and physiological conditions corresponds to *dry skin* model. As expected, the complex permittivity of *wet skin* is higher than that of *dry skin*.

TABLE I
Overview of the Skin Dielectric Properties at 60 GHz

Reference	Complex permittivity ε^*	T, °C	Method	Sample type
Gandhi *et al.* [30]	$8.89 - j13.15$	37±0.5	E	*In vitro*
Alabaster *et al.* [31]	$9.9 - j9.0$	23	M	*In vitro*
Gabriel *et al.* [32] "wet skin"	$10.22 - j11.84$	37	E	*In vitro*
Gabriel *et al.* [32] "dry skin"	$7.98 - j10.90$	32.5±0.5	E	*In vivo*
Alekseev *et al.* [33]	$8.12 - j11.14$	32.5±0.3	M	*In vivo*
Chahat *et al.* [34]	$8.4 - j10.96$	32.5±0.5	M	*In vivo*
Our model	$8.02 - j10.5$	32.5±0.5	M	*In vivo*

E = Extrapolation. M = Measurement.

Alekseev and Zizkin [33] performed *in vivo* reflection measurements using an open-ended waveguide and proposed homogeneous and multilayer human skin models fitting the experimental data.

Using a new *in-vivo* measurement technique based on heating kinetics, we have characterized the skin dielectric properties [34] at MMWs. The penetration depth of skin reported in [34] equals 0.48 mm, which corresponds, following the methodology detailed in this paper, to the complex permittivity shown in Table I.

The first six lines of Table I provide a summary of the data previously reported at 60 GHz. These results show that the literature data vary significantly from one study to another depending on the sample type. Besides, since the skin consists of approximately 65% of free water [35], its complex permittivity is strongly dispersive and temperature dependent [36]; this should be also taken into account for definition of an accurate skin permittivity model.

Whereas the skin temperature under normal environmental conditions is around 32.5 °C, the skin permittivity of *in vitro* measurements is given for different temperatures, e.g., [30] and [31]. Besides, water content of *in vitro* skin samples might vary depending on the measurement protocol. Obviously, the most realistic skin permittivity models correspond to *in vivo* measurements (i.e., Gabriel *et al.* [32] (*dry skin*), Alekseev and Zizkin [33], and Chahat *et al.* [34]). It is worthwhile to note that these data are in a good agreement (Table I).

To validate our measurement technique and obtain reference data for the skin-equivalent phantom, we performed a measurement campaign on a group of volunteers.

B. Setup for Permittivity Measurements

The experimental setup implemented to measure the complex permittivity of the human skin (Fig. 1) includes: 1) an Agilent 8510C 45-MHz–110-GHz vector network analyzer (VNA) operated by a PC with Agilent 85070 software through the Agilent 82357A GPIB interface; 2) an Anritsu 3670V50 coaxial cable (dc–70 GHz); and 3) an open-ended coaxial slim probe. This probe has been recently designed by Agilent Technologies, Santa Clara, CA, for permittivity measurements of lossy liquids

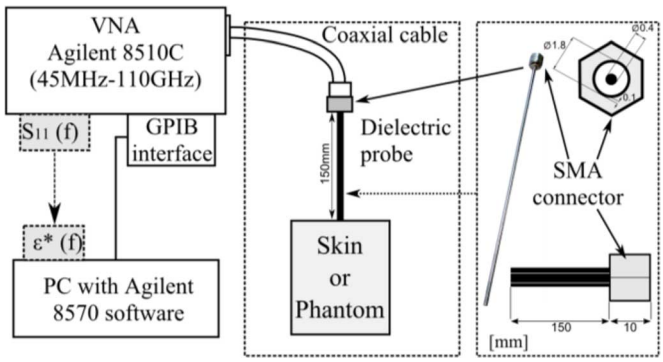

Fig. 1. Experimental setup used to measure the skin permittivity.

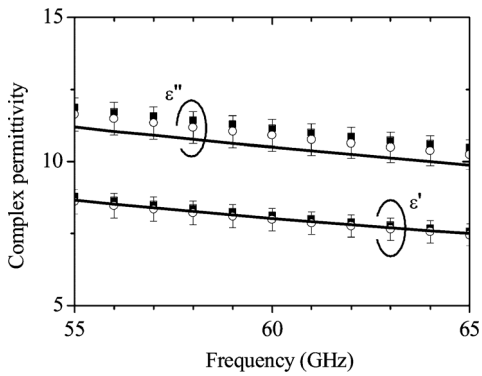

Fig. 2. Comparison of our experimental result for the wrist skin permittivity (▬) with Gabriel *et al.* (dry skin) (■) and Alekseev and Ziskin (○) models. Error bars represent ±5% deviations around Gabriel's reference values.

and semisolids up to 67 GHz. The accuracy of this tool has been recently demonstrated [37].

Before measuring the skin permittivity, the experimental setup is calibrated using three standard materials, namely, the surrounding air, a short circuit, and distilled water with known complex permittivity. Specific care has been taken to ensure a perfect contact between the probe tip and the sample under test to avoid any air gap that could alter the measurement accuracy. All experiments have been performed under normal environmental conditions. A Reflex optical fiber thermometer (NEOPTIX, Québec, QC, Canada) with a reproducibility of ±0.05 °C and accuracy of ±0.5 °C have been used to monitor locally the temperature of samples.

C. Measurements of the Human Skin Permittivity

The skin permittivity ($\varepsilon^* = \varepsilon' - j\varepsilon''$) has been measured on seven subjects at two specific locations, namely, the wrist and forearm. All volunteers were informed about the purpose of the measurements and have a solid background in electromagnetics. Four measurements have been performed with the same calibration at each location and for each volunteer. Thus, 28 measurements are available in total for each location. The skin temperature is equal to 32.5 ± 0.5 °C.

Measurements performed from 55 to 65 GHz have demonstrated very small variations between the skin permittivities at wrist and forearm (difference lower than 4%). Therefore, only one model defined by the average of all measurements performed at wrist is considered here. It is represented in Fig. 2

TABLE II
POWER REFLECTION COEFFICIENT, PD, AND SAR IN THE SKIN FOR DIFFERENT DIELECTRIC MODELS AT 60 GHz (INCIDENT PD = 1 mW/cm²)

Model	Power reflection coefficient, %	Max. PD, *mW/cm²*	Max. SAR, *W/kg*	Penetration depth, *mm*
Gandhi *et al.* [30]	41.2	0.59	25.4	0.43
Alabaster *et al.* [31]	35.7	0.64	19.6	0.60
Gabriel *et al.* [32] "wet skin"	39.7	0.60	22.9	0.48
Gabriel *et al.* [32] "dry skin"	37.8	0.62	23.9	0.48
Alekseev *et al.* [33]	38.2	0.62	24.0	0.47
Chahat *et al.* [34]	37.9	0.62	23.5	0.48
Our model (Fig. 2)	37.1	0.63	23.4	0.49

and compared with Gabriel *et al.* [32] and Alekseev and Ziskin [33] data. A very good agreement is demonstrated for the three data sets. The absolute deviations compared to Gabriel's data at 60 GHz are 0.5% and 3.7% for the real and imaginary parts, respectively. It is worthwhile to note that these results are different from the skin permittivity model previously reported by our research team [38] as here an improved calibration procedure has been used [34]. However, the data reported here have been also recently confirmed using the measurement technique based on the heating kinetic [34], as shown in Table I.

The measured skin permittivity can be described by a Debye equation with a single relaxation time τ equal to that of free water at the same temperature [33]

$$\varepsilon^* = \varepsilon_\infty + \frac{\Delta\varepsilon}{1 + j\omega\tau} + \frac{\sigma}{j\omega\varepsilon_0}. \quad (1)$$

In this equation, $\omega = 2\pi f$, f [Hz] is the frequency, $\Delta\varepsilon = \varepsilon_s - \varepsilon_\infty$ is the magnitude of the dispersion of the free water fraction of skin, ε_s is the permittivity at $\omega\tau \ll 1$, ε_∞ is the optical permittivity, $\varepsilon_0 = 8.85 \cdot 10^{-12}$ F/m, and σ [S/m] is the ionic conductivity. The optimized parameters that fit to the measured permittivity in the 55–65-GHz range are the following: $\varepsilon_\infty = 4.1, \varepsilon_s = 34.8, \tau = 6.9 \times 10^{-12}$ s, and $\sigma = 0.7$ S/m. The graphical representation of this model is not provided as a perfect fit with the experimental data is obtained over 55–65-GHz range. These Debye parameters are necessary for an accurate representation of the skin dielectric properties in electromagnetic software such as CST MWS or SEMCADX.

D. Influence of Small Variations of the Skin Permittivity on the Reflection/Transmission, PD, and SAR

Here we analytically investigate the impact of the differences between the skin permittivity models given in Table I upon: 1) reflection from the skin under normal incidence; 2) peak power density (PD) and peak SAR on the skin surface; and 3) penetration depth. The results are provided in Table II for a semi-infinite homogeneous skin model with a density of 1090 kg/m^3. They demonstrate a very good agreement for all considered parameters calculated for our, Gabriel *et al.*, and Alekseev and Ziskin models.

The attenuation of the PD within skin is plotted in Fig. 3 for an incident PD of 1 mW/cm^2. Again, very slight differences are observed between our, Gabriel *et al.*, and Alekseev and Ziskin models. At 1 mm under the skin surface, the absorbed power is

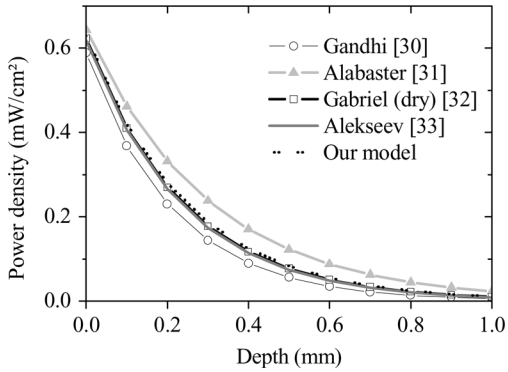

Fig. 3. Attenuation of the PD in the skin for an incident PD of 1 mW/cm^2 at 60 GHz and for different dielectric models.

attenuated by more than 98%. This means that the thickness of the phantom can be limited to several millimeters in practice.

III. Skin-Equivalent Phantom in the 55–65-GHz Range

A. Composition of the Phantom

The main components employed for the fabrication of the proposed semisolid skin-equivalent phantom are the following.

1) *Deionized water*. Water is the main constituent of the phantom because it is also the main skin component [35]. It primarily determines the dispersive behavior of the phantom.
2) *Agar*. It is employed for the retention of self-shaping, and its contribution to the phantom dielectric properties is negligible for small concentrations (typically below 4%) [34].
3) *Polyethylene powder*. It is used to tune the real and imaginary parts of the phantom permittivity.
4) *TX-151*. Since the agar and polyethylene powder cannot be mixed directly, the viscosity is increased using TX-151.
5) *Sodium azide*(NaN_3). It serves as a preservative.

B. Phantom Fabrication

The fabrication steps are the following. Deionized water, sodium azide, and agar are mixed in a kettle and heated on a stove, while the mixture is continuously stirred. When this liquid starts boiling, heating is stopped. TX-151 is sprinkled into the liquid and quickly mixed. The polyethylene powder is then added into the stirred liquid. Finally, the obtained mixture is poured into a mold and cooled in the same container for a few hours to room temperature for solidification. Using alginate gel powder, molds with realistic body-specific shapes can be manufactured for the phantom fabrication, as illustrated in Fig. 4.

Particular attention should be paid to the following critical points. First, to avoid strong dielectric deviation from one phantom to another, the room temperature should remain identical (in our case, 20 ± 1 °C) during the fabrication and further measurements. Second, the type of polyethylene powder is important; we recommend using particles with an average diameter of 20 μm and low density $\sim$900–1100 kg/m^3. Finally, to preserve the dielectric properties of the phantom over time, it is important to avoid water evaporation since this would result in a decrease of the permittivity. This can be for instance achieved by wrapping the phantom in a plastic film.

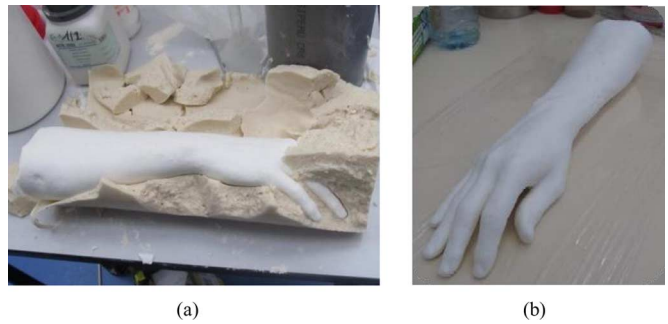

Fig. 4. Skin-equivalent phantom representing an arm and a hand. (a) Solidified phantom in an alginate mold. (b) Final phantom several hours after fabrication.

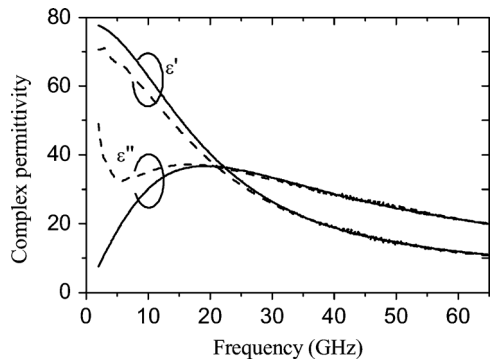

Fig. 5. Comparison between the complex permittivity of distilled water (——) and a saline (NaCl) solution (– –) at 20 °C.

C. Adjustment of the Electrical Properties of the Phantom

Similar components have been used for the fabrication of phantoms below 11 GHz [23]. At these frequencies, sodium chloride (NaCl) is commonly used to increase the imaginary part of the permittivity. However, at MMWs, the use of NaCl is meaningless, as the ionic conductivity does not affect the complex permittivity above 25 GHz. This is demonstrated in Fig. 5 where the complex permittivity of an NaCl solution (0.5 mol/L) is compared to the one of distilled water.

At MMWs, the complex permittivity of the phantom can be adjusted by tuning the concentration of the polyethylene powder (Fig. 6). The best fit with our model is obtained for a concentration of polyethylene powder of 20%. The amount of Agar and TX-151 has been optimized to obtain a homogeneous semisolid phantom for this amount of polyethylene powder. The composition leading to the best agreement with the reference permittivity values is given in Table III, and the corresponding permittivity of the phantom in the 55–65-GHz range is represented in Fig. 7. The phantom permittivity measured at 60 GHz equals to $\varepsilon^* = 7.4 - j11.4$. Compared to the measured skin values, errors of 7.7% and 8.6% are found, respectively, for the real and imaginary part of the permittivity, whereas they respectively equal to 7.3% and 4.6% compared to Gabriel *et al.* data.

These small deviations are acceptable for antenna measurement and dosimetric studies since they lead to negligible variations of the power reflection coefficient at the phantom/air in-

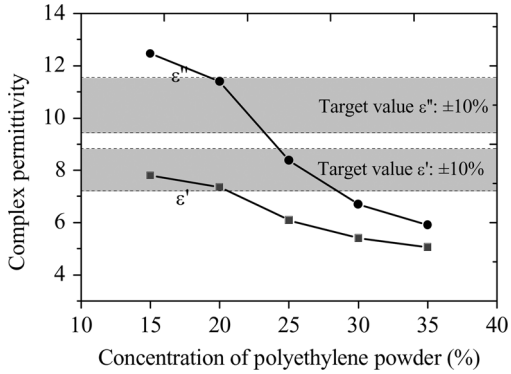

Fig. 6. Dielectric properties of phantoms at 60 GHz for different concentrations of polyethylene powder at 20 °C. Target values correspond to the measured permittivity of skin (see Section II.C).

TABLE III
COMPOSITION OF THE PROPOSED SKIN-EQUIVALENT PHANTOM

Ingredients	Mass, *g*
Deionized water	200
Agar	3
Polyethylene powder	40
TX-151	4
Sodium azide	0.2

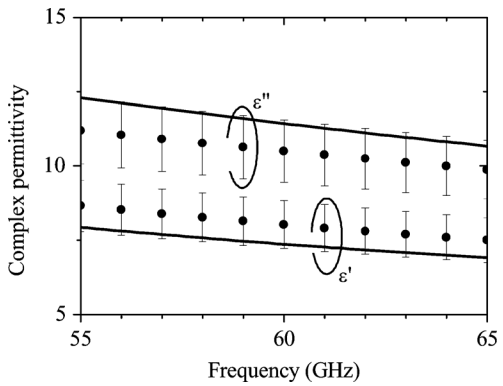

Fig. 7. Measured skin permittivity (•) and dielectric properties of the proposed phantom (▬) in the 55–65-GHz range. Error bars represent ±10% of the measured skin permittivity.

terface (1.4% for the normal incidence at 60 GHz) and of the penetration depth (8%) compared to skin.

Furthermore, they result in SAR deviations of only 6.8% and 4.5% compared to the measured skin permittivity and Gabriel *et al.* data, respectively. As similar variations are experienced for different locations on the body and due to the inter-individual changes (because of the difference of water concentration in tissues), this phantom can be used successfully as a representative body surface model for antenna measurement, on-body channel characterization, and determination of the power absorption in the body.

It is worthwhile to note that the accuracy of this phantom is sufficient for dosimetric studies and similar to the one of phantoms developed at microwaves. For instance, the phantom proposed in [24] shows discrepancies of ±10% within the 3.1–10.6-GHz range, the broadband tissue-equivalent liquid [22] shows variations of ±11% within the 0.3–6-GHz range, and the carbon–silicone phantom [27] properties fall within ±15% of the target values in the 0.6–6-GHz range.

Finally, in order to assess the life time of the proposed phantoms, it was wrapped in a plastic film, placed in a plastic case to prevent from drying, and kept at room temperature for four weeks. The complex permittivity of the phantom was measured once a week during one month. No significant change was observed, confirming thereby the stability of the phantom.

Other solutions could be explored to obtain more accurate dielectric and/or mechanical properties. For instance, it would be interesting to investigate the feasibility of carbon phantom in the millimeter-wave band [26], [27]. However, such phantoms require special and expensive equipment whereas the proposed phantom is inexpensive, easy to fabricate in laboratory environments, and provides sufficient accuracy for reliable on-body antenna measurements and dosimetric studies.

IV. VALIDATION OF THE PHANTOM BY SAR MEASUREMENTS

To confirm the relevance of the proposed skin-equivalent phantom for experimental dosimetry, the SAR is measured on the phantom surface using an infrared (IR) camera.

A. Setup for SAR Measurements

The experimental setup developed for SAR measurements is similar to that presented in [34]. A cylindrical phantom with a thickness of 1 cm and a diameter of 14 cm is exposed at 60 GHz using a WR-15 open-ended rectangular waveguide located at 15 mm above the phantom. A continuous-wave signal is generated at 60 GHz by a narrowband Gunn oscillator. This signal is amplified and transmitted towards the open-ended waveguide used as an antenna through a set of WR-15 waveguides. Here the input power $P_{\rm in}$ of the antenna equals 500 mW. It was controlled and adjusted before each experiment using an Agilent E4418B power meter (Agilent Technologies).

An FLIR SC5000 high-resolution infrared (IR) camera (FLIR Systems, Portland, OR) operating in the 2.5–5.1-μm spectral range is used for recording the heating pattern and dynamics on the phantom surface. The thermal sensitivity of the camera equals 0.025 °C. The sequence of the thermal images is recorded at 25 frames/s rate with a spatial resolution of 640 × 512 pixels.

B. SAR Determination

The SAR is proportional to the initial temperature rise rate and can be determined as follows [29]:

$$\mathrm{SAR}_0 = C\left.\frac{dT}{dt}\right|_{t=0} \tag{2}$$

where C is the specific heat [J/(kg · K)], dT is the temperature rise [°C], and dt is the heating time [s]. The most accurate way to determine $dT/dt|_{t=0}$ is to fit the experimental heating kinetics to an appropriate theoretical thermal model [29].

To determine the peak surface SAR on the phantom surface, the experimental results Fig. 8(a) are fitted to the theoretical solution of the 1-D bio-heat transfer equation [39], assuming that the thermal conductivity, specific heat, and density of the proposed phantom are equal to 0.5 W/(m·°C), 3.5 kJ/(kg·°C), and

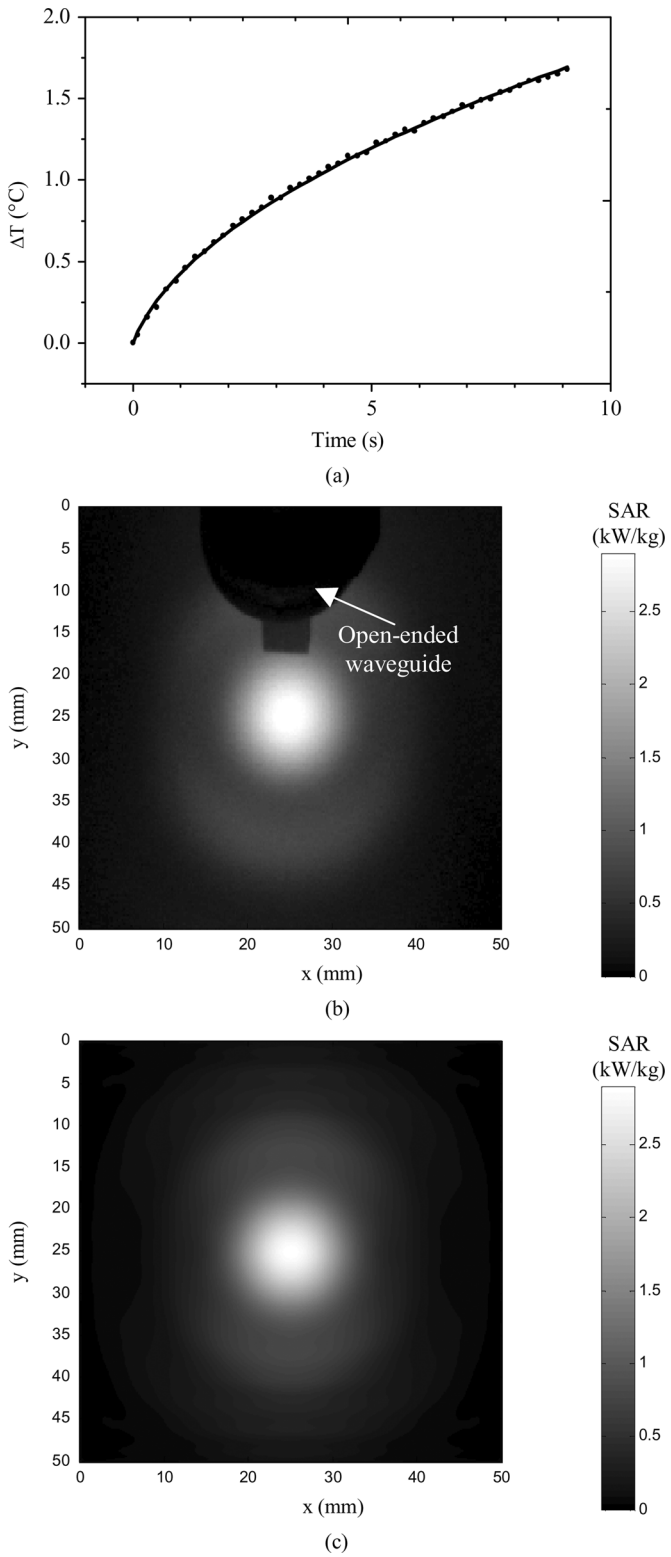

Fig. 8. (a) Temperature rise dynamics in the area of maximal temperature elevation: • • • experimental result, — theory (solution of the 1-D heat transfer equation). (b) Measured SAR distribution on the skin-equivalent phantom. (c) Simulated SAR distributions on the surface of the skin exposed at 60 GHz by an open-ended waveguide ($P_{\rm in} = 500$ mW).

880 kg/m^3 ($\rho_{\rm phantom}$), respectively. The fitting procedure consists in minimizing the standard deviation value between the experimental heating kinetics and the theoretical one. The corresponding results are plotted in Fig. 8(a).

The tissue-equivalent phantom possesses a density, which is different from that of actual skin tissue ($\rho_{\rm skin} = 1090$ kg/m^3). Consequently, the SAR estimated in the skin-equivalent phantom, $\mathrm{SAR}_{\rm phantom}$, using the phantom density $\rho_{\rm phantom}$, differs from the SAR that would occur in the skin, $\mathrm{SAR}_{\rm skin}$. Hence, the relationship $\mathrm{SAR}_{\rm skin} = \rho_{\rm phantom}/\rho_{\rm skin} \cdot \mathrm{SAR}_{\rm phantom}$ yields the SAR in the skin [40].

The measured Fig. 8(b) and computed Fig. 8(c) SAR distributions are in very good agreement. In particular, the measured peak SAR equals 3.01 kW/kg, whereas the value computed using CST Microwave Studio is 2.97 kW/kg (relative deviation $\Delta = 1.3\%$). These results confirm that the proposed phantom can be employed successfully for SAR measurement.

V. Conclusion

A semisolid broadband skin-equivalent phantom has been designed and fabricated in order to emulate the permittivity values of human skin in V-band. It can be used for on-body antenna measurements and propagation channel characterization for BAN, as well as for electromagnetic dosimetry studies in the 55–65-GHz range.

First, the dielectric properties of the human skin have been measured *in vivo* using a coaxial slim probe. An excellent agreement was demonstrated with other reported skin models in the 55–65-GHz range.

Second, a water-based skin-equivalent phantom has been designed using our measured human skin permittivity values as a reference. This phantom has been manufactured using deionized water, agar, polyethylene powder, TX-151, and sodium azide. The maximum deviations of the phantom permittivity with respect to the human skin are of 7.7% (real part) and 8.6% (imaginary part) at 60 GHz. They are below 10% in the 55–65-GHz range. Such deviations are acceptable for antenna measurement and dosimetric studies since they lead to small variations of the power reflection coefficient, penetration depth, and SAR compared to skin.

Finally, SAR measurements have been performed using the proposed skin-equivalent phantom. An excellent agreement has been demonstrated between experimental and numerical results. This validates and confirms the very satisfactory characteristics of the proposed phantom.

References

[1] P. S. Hall and Y. Hao, *Antennas and Propagation for Body Centric Communications Systems*. Norwood, MA: Artech House, 2006.

[2] D. Guha and Y. M. M. Antar, *Microstrip and Printed Antennas: New Trends, Techniques and Applications*. New York: Wiley, 2011.

[3] C. Hertleer, H. Rogier, L. Vallozzi, and L. Van Langenhove, "A textile antenna for off-body communication integrated into protective clothing for firefighters," *IEEE Trans. Antennas Propag.*, vol. 57, no. 4, pp. 919–925, Apr. 2009.

[4] C. Hertleer, A. Tronquo, H. Rogier, L. Vallozzi, and L. Van Langenhove, "Aperture-coupled patch antenna for integration into wearable textile systems," *IEEE Antennas Wireless Propag. Lett.*, vol. 6, pp. 392–395, 2007.

[5] N. Chahat, M. Zhadobov, R. Sauleau, and K. Ito, "A compact UWB antenna for on-body applications," *IEEE Trans. Antennas Propag.*, vol. 59, no. 4, pp. 1123–1131, Apr. 2011.

[6] A. Alomainy, Y. Hao, C. G. Parini, and P. S. Hall, "Comparison between two different antennas for UWB on-body propagation measurements," *IEEE Antennas Wireless Propag. Lett.*, vol. 4, pp. 31–34, 2005.

[7] N. Haga, K. Saito, M. Takahashi, and K. Ito, "Characteristics of cavity slot antenna for body-area networks," *IEEE Trans. Antennas Propag.*, vol. 57, no. 4, pp. 837–843, Apr. 2009.
[8] P. S. Hall, Y. Hao, Y. I. Nechayev, A. Alomalny, C. C. Constantinou, C. Parini, M. R. Kamarudin, T. Z. Salim, D. T. M. Hee, R. Dubrovka, A. S. Owadally, W. Song, A. Serra, P. Nepa, M. Gallo, and M. Bozzetti, "Antennas and propagation for on-body communication systems," *IEEE Antennas Propag. Mag.*, vol. 49, no. 3, pp. 41–58, Jun. 2007.
[9] Q. H. Abbasi, A. Sani, A. Alomainy, and Y. Hao, "Arm movements effect on ultra wideband on-body propagation channels and radio systems," in *Antennas Propag. Conf.*, Loughborough, U.K., Nov. 2009, pp. 261–264.
[10] Q. Abbasi, A. Alomainy, and Y. Hao, "Effect of human body movements on performance of multiband OFDM based ultra wideband wireless communication system," in *Antennas Propag. Conf.*, Loughborough, U.K., Nov. 2010, pp. 145–148.
[11] I. Khan, P. S. Hall, A. A. Serra, A. R. Guraliuc, and P. Nepa, "Diversity performance analysis for on-body communication channels at 2.45 GHz," *IEEE Trans. Antennas Propag.*, vol. 57, no. 4, pp. 956–963, Apr. 2009.
[12] S. Cheng, E. Ojefors, P. Hallbjorner, S. Ogden, J. Margell, K. Hjort, and A. Rydberg, "Body surface backed flexible antennas for 17 GHz wireless body area networks sensor applications," in *Eur. Wireless Technol. Conf.*, Amsterdam, The Netherland, Oct. 2007, pp. 55–58.
[13] G. A. Conway and W. G. Scanlon, "Antenna for over-body-surface communication at 2.45 GHz," *IEEE Trans. Antennas Propag.*, vol. 57, no. 4, pp. 844–855, Apr. 2009.
[14] S. Zhu and R. Langley, "Dual-band wearable textile antenna on an EBG substrate," *IEEE Trans. Antennas Propag.*, vol. 57, no. 4, pp. 926–935, Apr. 2009.
[15] Q. Wang, T. Tayamachi, I. Kimura, and J. Wang, "An on-body channel model for UWB body area communications for various postures," *IEEE Trans. Antennas Propag.*, vol. 57, no. 4, pp. 991–998, Apr. 2009.
[16] S. L. Cotton, W. G. Scanlon, and B. K. Madahar, "Millimeter-wave soldier-to-soldier communications for covert battlefield operations," *IEEE Commun. Mag.*, vol. 47, no. 10, pp. 72–81, Oct. 2009.
[17] X. Y. Wu and P. S. Hall, "Substrate integrated wavegide Yagi–Uda antenna," *Electron. Lett.*, vol. 11, no. 23, pp. 1541–1542, Nov. 2010.
[18] X. Y. Wu, L. Akhoondzadeh-Asl, and P. S. Hall, "Printed Yagi–Uda array for on-body communication channels at 60 GHz," *Microw. Opt. Technol. Lett.*, vol. 53, no. 12, pp. 2728–2730, Dec. 2011.
[19] M. Zhadobov, N. Chahat, R. Sauleau, C. Le Quément, and Y. Le Dréan, "Millimeter-wave interactions with the human body: State of knowledge and recent advances," *Int. J. Microw. Wireless Technol.*, vol. 3, no. 2, pp. 237–247, 2011.
[20] C. Gustafson and F. Tufvesson, "Characterization of 60 GHz shadowing by humanbodies and simple phantoms," in *Eur. Antennas Propag. Conf.*, Prague, Czech Republic, Mar. 26–30, 2012, Sec. P09.
[21] N. Chahat, M. Zhadobov, R. Sauleau, and K. Mahdjoubi, "Variability analysis of on-body antenna characteristics for different adult and child voxel models," in *Eur. Antennas Propag. Conf.*, Rome, Italy, Apr. 11–15, 2010, pp. 437–440.
[22] "MCL-T broadband tissue equivalent liquid: 30 MHz to 6 GHz," MCL-T, London, U.K. [Online]. Available: http://www.mcluk.org/pdfs/bbl.pdf
[23] K. Ito, K. Furuya, Y. Okano, and L. Hamada, "Development and characteristics of a biological tissue-equivalent phantom for microwaves," *Electron. Commun. Japan*, vol. 84, no. 4, pp. 67–77, Apr. 2001.
[24] T. Takimoto, T. Onishi, K. Saito, M. Takahashi, S. Uebayashi, and K. Ito, "Characteristics of biological tissue equivalent phantoms applied to UWB communications," *Electron. Commun. Japan*, vol. 90, no. 5, pp. 48–55, May 2007.
[25] J. Yonebayashi, S. Takamatsu, K. Saito, M. Takahashi, and K. Ito, "Development of dynamic phantom for evaluation of breath detection Doppler radar," in *32nd Annu. Bioelectromagn. Soc. Meeting*, Seoul, Korea, Jun. 2010, pp. 297–299.
[26] T. Kobayashi, T. Nojima, K. Yamada, and S. Uebayashi, "Dry phantom composed of ceramics and its application to SAR estimation," *IEEE Trans. Microw. Theory Tech.*, vol. 41, no. 1, pp. 136–140, Jan. 1993.
[27] C. Gabriel, "Tissue equivalent material for hand phantoms," *Phys. Med. Biol.*, vol. 53, no. 14, pp. 4205–4210, Jul. 2007.
[28] N. Chahat, M. Zhadobov, S. Alekseev, and R. Sauleau, "Human skin-equivalent phantom for on-body antenna measurements in the 60-GHz band," *Electron. Lett.*, vol. 48, no. 2, pp. 67–68, Jan. 2012.
[29] S. I. Alekseev and M. C. Ziskin, "Local heating of human skin by millimeter waves: A kinetics study," *Bioelectromagnetics*, vol. 24, no. 8, pp. 571–581, Oct. 2003.
[30] O. P. Gandhi and A. Riazi, "Absorption of millimeter waves by human beings and its biological implications," *IEEE Trans. Microw. Theory Tech.*, vol. MTT-34, no. 2, pp. 228–235, Feb. 1986.
[31] C. M. Alabaster, "Permittivity of human skin in millimetre wave band," *Electron. Lett.*, vol. 39, no. 21, pp. 1521–1522, Oct. 2003.
[32] S. Gabriel, R. W. Lau, and C. Gabriel, "The dielectric properties of biological tissues: III. Parametric models for the dielectric spectrum of tissues," *Phys. Med. Biol.*, vol. 41, no. 11, pp. 2271–2293, Nov. 1996.
[33] S. I. Alekseev and M. C. Ziskin, "Human skin permittivity determined by millimeter wave reflection measurements," *Bioelectromagnetics*, vol. 28, no. 5, pp. 331–339, Jul. 2007.
[34] N. Chahat, M. Zhadobov, R. Sauleau, and S. I. Alekseev, "New method for determining dielectric properties of skin and phantoms at millimeter waves based on heating kinetics," *IEEE Trans. Microw. Theory Tech.*, vol. 60, no. 3, pp. 827–832, Mar. 2012.
[35] F. A. Duck, *Physical Properties of Tissues*. Bath, U.K.: Academic, 1990.
[36] R. Buchner, J. Barthel, and J. Stauber, "The dielectric relaxation of water between 0°C and 35°C," *Chem. Phys. Lett.*, vol. 306, no. 1–2, pp. 57–63, Jun. 1999.
[37] M. Zhadobov, R. Augustine, R. Sauleau, A. Di Paola, C. Le Quément, Y. Soubere Mahamoud, and Y. Le Dréan, "Complex permittivity of representative biological solutions in the 2–67 GHz range," *Bioelectromagnetics*, vol. 33, no. 4, pp. 346–355, May 2012.
[38] N. Chahat, M. Zhadobov, R. Augustine, and R. Sauleau, "Human skin permittivity models for millimetre-wave range," *Electron. Lett.*, vol. 47, no. 7, pp. 427–428, Mar. 2011.
[39] K. R. Foster, H. N. Kritikos, and H. P. Schwan, "Effect of surface cooling and blood flow on the microwave heating of tissue," *IEEE Trans. Biomed. Eng.*, vol. 25, no. 3, pp. 313–316, May 1978.
[40] *IEEE Recommended Practice for Determining the Peak Spatial-Average Specific Absorption Rate (SAR) in the Human Head From Wireless Communications Devices: Measurement Techniques*, IEEE Standard 1528-2003, 2003.

Nacer Chahat (S'09) was born in Angers, France, in 1986. He received the Electrical Engineering and Radio Communications degree from the Ecole Supérieur d'ingénieurs de Rennes (ESIR), Rennes, France, in 2009, the Master's Degree in telecommunication and electronics from the University of Rennes 1, Rennes, France, in 2009, and is currently working toward the Ph.D. degree in signal processing and telecommunications at the Institute of Electronics and Telecommunications of Rennes (IETR), University of Rennes 1.

His current research fields are electrically small antennas, millimeter-wave antennas, and the evaluation of the interaction between the electromagnetic field and human body. In 2009, he completed a six-month master's training period as a special research student at the Graduate School of Engineering, Chiba University, Chiba, Japan.

Mr. Chahat was the recipient of the 2011 Best Paper Award from the Bioelectromegnetics Society, the 2011 CST University Publication Award, and the 2012 IEEE Antenna and Propagation Society Doctoral Research Award.

Maxim Zhadobov (S'05–M'07) received the M.S. degree in radiophysics from Nizhni Novgorod State University, Nizhni Novgorod, Russia, in 2003, and the Ph.D. degree in bioelectromagnetics from the Institute of Electronics and Telecommunications of Rennes (IETR), University of Rennes 1, Rennes, France, in 2006.

In 2008, he completed post-doctoral training with the Center for Biomedical Physics, Temple University, Philadelphia, PA. He then rejoined IETR as an Associate Scientist with the Centre National de la Recherche Scientifique (CNRS). He has authored or coauthored over 80 scientific papers. His main scientific interests are in the field of biocompatibility of electromagnetic radiations, including interactions of microwaves, MMWs and pulsed radiations at the cellular and sub-cellular levels, health risks and environmental safety of emerging wireless communication systems, biocompatibility of wireless noninvasive biomedical techniques, bioelectromagnetic optimization of body-centric wireless systems, experimental and numerical

electromagnetic dosimetry, and therapeutic applications of nonionizing radiations.

Dr. Zhadobov was the recipient of the 2005 Best Poster Presentation Award from the International School of Bioelectromagnetics, the 2006 Best Scientific Paper Award from the Bioelectromegnetics Society, and Brittany's Young Scientist Award in 2010.

Ronan Sauleau (M'04–SM'06) received the Electrical Engineering and Radio Communications degree from the Institut National des Sciences Appliquées, Rennes, France, in 1995, the Agrégation degree from the Ecole Normale Supérieure de Cachan, Cachan, France, in 1996, and the Doctoral degree in signal processing and telecommunications and Habilitation à Diriger des Recherche degree from the University of Rennes 1, Rennes, France, in 1999 and 2005, respectively.

From September 2000 to November 2005 and December 2005 to October 2009, he was an Assistant Professor and Associate Professor, respectively, with the University of Rennes 1. Since November 2009, he has been a Full Professor with the University of Rennes 1. He has authored or coauthored over 100 journal papers and 240 contributions to national and international conferences and workshops. He holds five patents. His current research fields are numerical modeling [mainly finite difference time domain (FDTD)], millimeter-wave printed and reconfigurable [microelectromechanical systems (MEMS)] antennas, lens-based focusing devices, periodic and nonperiodic structures (electromagnetic-bandgap materials, metamaterials, reflect arrays, and transmit arrays), and biological effects of MMWs.

Prof. Sauleau was the recipient of the 2004 ISAP Conference Young Researcher Scientist Fellowship (Japan) and the first Young Researcher Prize in Brittany, France, in 2001 for his research on gain-enhanced Fabry–Perot antennas. In September 2007, he was elevated to Junior Member of the Institut Universitaire de France. He was also the recipient of the Bronze Medal of the CNRS in 2008.